Photochemical creation of covalent organic 2D monolayer objects in defined shapes via a lithographic 2D-polymerization

Servalli, M.; Celebi, K.; Payamyar, P.; Zheng, L.; Polozij, M.; Lowe // , B.; Kuc, A.; Schwarz, T.; Thorwarth, K.; Borgschulte○, A.; Heine, T.; Zenobi, R.; Schlüter, A. D.;

Originally published:

October 2018

ACS Nano 12(2018)11, 11294-11306

DOI: https://doi.org/10.1021/acsnano.8b05964

Article

Photochemical Creation of Covalent Organic 2D Monolayer Objects in Defined Shapes *via* a Lithographic 2D-Polymerization

Marco Servalli, Kemal Celebi, Payam Payamyar, Liqing Zheng, Miroslav Polozij, Benjamin Lowe, Agnieszka Kuc, Tobias Schwarz, Kerstin Thorwarth, Andreas Borgschulte, Thomas Heine, Renato Zenobi, and A. Dieter Schlüter

ACS Nano, **Just Accepted Manuscript** • DOI: 10.1021/acsnano.8b05964 • Publication Date (Web): 16 Oct 2018

Photochemical Creation of Covalent Organic 2D Monolayer Objects in Defined Shapes *via* a Lithographic 2D-Polymerization

Marco Servalli[†*], Kemal Celebi[†], Payam Payamyar[‡], Liqing Zheng[§], Miroslav Položij[∥#], Benjamin Lowe[∥], Agnieszka Kuc[∥¶], Tobias Schwarz[◊], Kerstin Thorwarth[○], Andreas Borgschulte[○], Thomas Heine[∥#¶], Renato Zenobi[§], A. Dieter Schlüter[†]

[†]Laboratory of Polymer Chemistry, Department of Materials, ETH Zurich, Vladimir-Prelog-Weg 5, 8093 Zurich, Switzerland

[‡]John A. Paulson School of Engineering and Applied Sciences, Harvard University, 9 Oxford Street, Cambridge, MA 02138

[§]Laboratory of Organic Chemistry, Department of Chemistry and Applied Biosciences, ETH Zurich, Vladimir-Prelog-Weg 3, 8093 Zurich, Switzerland

[∥]Wilhelm-Ostwald-Institut für Physikalische und Theoretische Chemie, Universität Leipzig, Linnéstrasse 2, 04103 Leipzig, Germany

[#]Technische Universität Dresden, Theoretische Chemie, Bergstraße 66b, 01062 Dresden, Germany

[¶]Helmholtz-Zentrum Dresden-Rossendorf, Abteilung Ressourcenökologie, Forschungsstelle Leipzig, Permosenstrasse 15, 04318 Leipzig, Germany

[◊]ScopeM, Institute of Biochemistry, ETH Zurich, Otto-Stern-Weg 3, 8093 Switzerland

[○]Empa, Swiss Federal Laboratories for Materials Science and Technology, Advanced Analytical Technologies, Überlandstrasse 129, 8600 Dübendorf, Switzerland

ABSTRACT: In this work we prepare Langmuir-Blodgett monolayers with a trifunctional amphiphilic anthraphane monomer. Upon spreading at the air/water interface, the monomers self-assemble into 1 nm-thin monolayer islands, which are highly fluorescent and can be visualized by naked eye upon excitation. *In-situ* fluorescence spectroscopy indicates that in the monolayers, all the anthracene units of the monomers are stacked face-to-face forming excimer pairs, whereas at the edges of the monolayers free anthracenes are present acting as edge groups. Irradiation of the monolayer triggers [4+4]-cycloadditions among the excimer pairs, effectively resulting in a two-dimensional polymerization. The polymerization reaction also completely quenches the fluorescence, allowing to draw patterns on the monomer monolayers. More interestingly, after transferring the monomer monolayer on a solid substrate, by employing masks or the laser of a confocal scanning microscope, it is possible to arbitrarily select the parts of the monolayer that one wants to polymerize. The unpolymerized regions can then be washed away from the substrate, leaving two-dimensional macromolecular monolayer objects of the desired shape. This photolithographic process employs 2D-polymerizations and affords 1 nm-thin coatings.
KEYWORDS: *self-assembled monolayers, fluorescence, air/water interface, anthracene, photolithography, 2D polymerization*

The interest for synthetic two-dimensional polymers (2DPs) is constantly on the rise due to their high degree of anisotropy, crystallinity, monolayer and organic nature.[1–4] Like other 2D materials such as graphene and transition metal dichalcogenides, 2D polymers present great promise in applications of societal relevance, such as ultra-thin membranes for molecular separation[5,6] and optoelectronic devices.[7–9] So far, two reliable methods have been developed for accessing 2DPs in our group: synthesis in single crystals and at the air/water interface. The first method ideally affords single crystals of stacked 2DPs through photochemically induced topochemical polymerizations.[10–14] Handling single crystals has the advantage of applying well established techniques for unequivocal structural characterization, such as single-crystal X-ray diffraction (SC-XRD), but in order to obtain the polymers as single-sheet entities, an exfoliation procedure is necessary, which more often than not results in thin sheet stacks rather than monolayers. Additionally, provided that the sheets do not rupture or fold during exfoliation, their maximal lateral extension is inherently limited by the lateral extension of the crystals themselves, which is typically in the sub-mm range. To overcome these limitations, we have been extensively engaged in the synthesis of 2DPs at the air/water interface,[15–20] where Langmuir-

Blodgett (LB) polymer monolayers of macroscopic size can be obtained. This technique has the advantage of directly yielding monolayers whose lateral extensions can, in principle, be tuned according to the lateral extension of the water surface employed. Yet, due to the small quantities of material involved (μg range), there is no fast, routine technique for structural characterization. Monolayer-sensitive spectroscopy techniques such as tip-enhanced Raman spectroscopy (TERS)[21,22] and X-ray photoelectron spectroscopy (XPS) are effective in characterizing the chemical nature of the sheets, however for assessing their structural periodicity diffracting techniques such as grazing-incidence small-angle X-ray scattering (GISAXS)[23] and selective area electron diffraction (SAED),[24,25] or direct imaging techniques such as atomic force microscopy (AFM) and scanning tunneling microscopy (STM) are necessary. The success of these techniques is highly dependent on the sample preparation, which for LB film requires a non-disruptive mechanical transfer of the soft nm-thin monolayer from the water surface onto suitable substrates. Recently, a 2DP was successfully prepared at the air/water interface and its structure was characterized by both STM and AFM,[26] however, over the years, a discrete number of organic covalent and metal-organic monolayers have been prepared,[15,18,27–31] whose structural periodicity has still to be unequivocally proven. Nevertheless, the lack of structural information did not hinder the pursuit of other interesting application-oriented avenues, which regard for instance the recently reported observation that it is possible to reversibly "write" into dense fluorescent monolayers on solid substrates with a confocal laser-scanning microscope (CLSM).[27] The writing process involves a photochemically triggered two-dimensional polymerization based on [4+4]-cycloaddition reactions between 1,8-diazaanthracene units of neighboring monomers. In the compressed monolayer, the 1,8-diazaanthracenes units are stacked face-to-face (*ftf*) in pairs and whenever they are excited by light, they form emittive excimers, which then decay to non-emittive diazaanthracene dimers. The dimerization reaction thus switches the fluorescence off, which causes the contrast required for writing.

This process is not only interesting because it causes contrast between irradiated and non-irradiated areas, but it is also significant because of its 'quantized' nature in a single molecule-thick layer. The monolayer can be viewed as an array of paired diazaanthracenes spatially separated from one another on the nm length scale. Once a dimer has formed, the newly formed structural element to a first approximation does not exert an influence on the adjacent unreacted neighboring anthracene pairs. In the language of polymer chemistry, this process therefore results in a step-growth rather than chain growth polymerization.[32,33] This differentiation has important implications. For example, it is the basis for the creation of monolayer 2D objects, whose shape and lateral extension are only dictated by up to which point the anthracene pairs are excited in a monomer array and do not depend on initiation and propagation sequences. This, in principle, could allow for a high level of control of the chemical structure of the edges of 2D objects as long as there is a mean to steer light excitation on the nm-scale *e.g.* by using interference[34] and immersion[35] lithographic techniques, maskless plasmonic lithography[36] or probe lithography using near-field scanning optical microscopy (NSOM) fiber probes.[37]

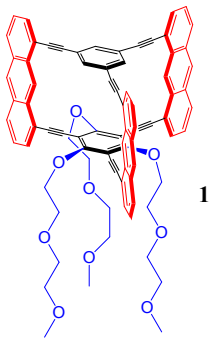

1

Figure 1. Chemical structure of the amphiphilic anthraphane **1** synthesized in this study. The monomer has a rigid hydrocarbon cyclophane scaffold bearing three anthracene photoreactive units (red); amphiphilicity is imparted by substituting one central benzene core with three diethylene glycol methyl ether (DEGME) groups (blue).

In this work we describe the synthesis of the amphiphilic anthraphane derivative **1** and its spreading behavior at an air/water interface. Compared to our previous studies, monolayers of **1** exhibit particularly high fluorescence intensity due to excimer formation. The possibility to induce a 2D-polymerization in selected areas of the monolayer will be explored both *in-situ* at the interface as well as *ex-situ,* after transferring the monolayer onto solid substrates such as silicon oxide, by using a hand-held violet laser pointer (405 nm) or the laser of a confocal fluorescence microscope (405 nm) to freely draw patterns or a home-built LED (385 nm) to imprint patterns by using masking techniques. Furthermore, it will be shown that non-irradiated parts of the monolayers can be removed from the solid substrate by simple solvent washing, leaving only the irradiated and polymerized patterned monolayer. This opens the intriguing possibility of using 2D polymerizations for photolithography, in which the monomer monolayer effectively acts as negative photoresist and can afford nm-thin coatings and patterns in the desired shapes.

The polymerization process will be investigated qualitatively and quantitatively by time-dependent *in-situ* fluorescence decay measurements, XPS and TERS, and the obtained conversion values will be corroborated by simple experiments showing the mechanical integrity of the polymerized monolayers due to bond percolation. These spectroscopical results, combined with surface pressure vs mean molecular area isotherm measurements at the air water/interface, will also be used to validate a DFT molecular model for the structure of the monomer and polymer monolayers at the air/water interface.

RESULTS AND DISCUSSION

Monomer synthesis. The desymmetrized amphiphilic structure of **1** was directly designed and adapted from the parent D_{3h}-symmetric hydrocarbon anthraphane[38] and from the desymmetrized anthraphane-tri(OMe),[39] whose crystal structures and photoreactivity were extensively investigated in single crystals.[40,41] Firstly, the polar benzene moiety was synthesized in three steps (Scheme 1):[42]

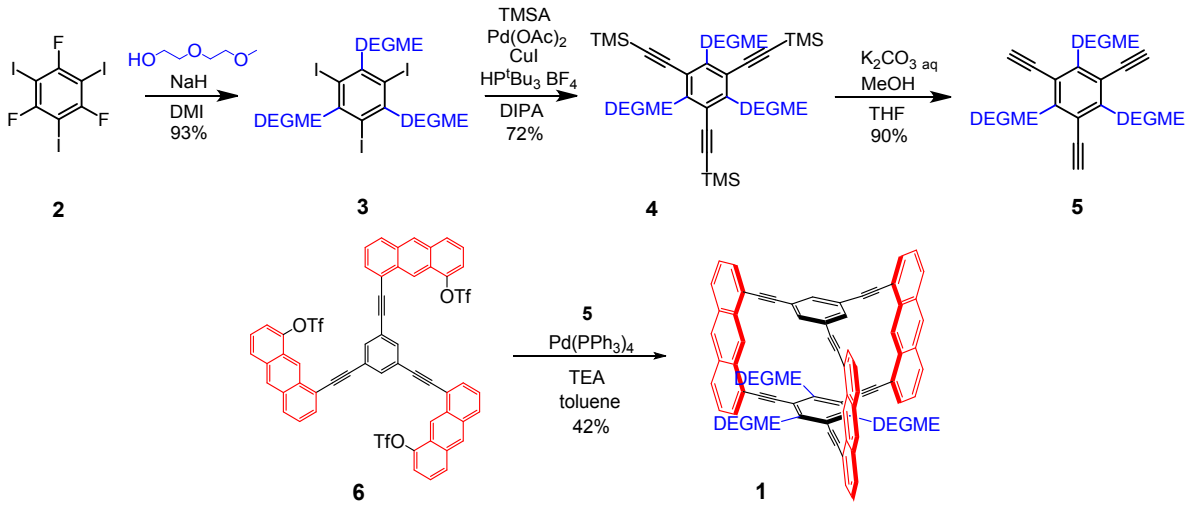

Scheme 1. Synthetic scheme of amphiphilic anthraphane 1. Synthesis of the diethylene glycol methyl ether-substituted benzene core 5 *(top)*; Modular synthesis of amphiphilic monomer 1 by copper-free Sonogashira cross-coupling between 5 and anthraphane precursor 6 *(bottom)*.

1,3,5-trifluorobenzene was quantitatively iodinated with periodic acid in sulfuric acid to give compound **2** in quantitative yields.[43] Triple nucleophilic aromatic substitution of the fluorides in anhydrous DMI with freshly prepared sodium 2-(2-methoxyethoxy)ethoxide yielded the substituted iodinated compound **3** in 93% yield. Sonogashira cross-coupling of **3** with trimethylsilylacetylene was performed with catalyst $Pd(P^tBu_3)_2$, which was generated *in-situ* from $Pd(OAc)_2$ and by deprotonation of $HP^tBu_3BF_4$ with diisopropylamine.[44] For such an electron-rich substrate, the reaction worked very well with yields up to 72%. In a final step, desylilation of **4** with potassium carbonate in methanol afforded quantitatively the target compound **5** in high purity and gram scale.

Monomer **1** was then assembled by copper-free Sonogashira cross-coupling between **5** and anthraphane precursor **6**. The crude target compound could be conveniently obtained by employing the same reaction conditions and work-up procedures used for the original anthraphane. Final recrystallization from boiling THF afforded **1** as pale yellow needles with yields up to 42% and in the 400 mg scale. The structure of **1** was unambiguously confirmed by high-resolution mass spectrometry (HRMS) and ^{1}H- and ^{13}C-NMR spectroscopy. Single crystals could be grown from a variety of solvents, such as chloroform, THF, DMSO, toluene, nitrobenzene and *o*-dichlorobenzene; however, while the main hydrocarbon skeleton of the monomer could be always identified in the crystal structures, the highly flexible diethylene glycol methyl ether (DEGME) chains were completely disordered and could not be modelled, always resulting in overall poorly resolved structures. In all the cases however, based on the fragmentary structure solutions, the monomer clearly packed tightly within layers, with the anthracene units in an exclusive edge-to-face (*etf*) relationship and with the DEGME chains folding back towards the anthracene units of the monomer rather than being extended and interpenetrating the layers (Figure S7).

Spreading at the air/water interface and molecular packing model. While not strictly necessary,[28,29] amphiphilicity can help to stabilize the conformation/orientation of molecules at the air/water interface (see SI page S43): compound **1** was expected to be oriented at the air/water interface with the polar moieties being in contact with the water subphase and the anthracenes standing vertically in the air. In the ideal case, upon compression or spontaneous self-assembly, monolayers of **1** were expected to pack into a hexagonal honeycomb-like structure through π-π stacking interactions between the anthracene units of the monomers. With all the anthracenes arranged in face-to-face (*ftf*) stacked pairs, upon photoexcitation excimers can be formed which then decay in covalently bonded anthracene dimers, forming a molecular fisherman's net.

A solution of **1** in a 1 : 1 chloroform/cyclohexane mixture (0.25 mg/mL) was spread at room temperature at the air/water interface in a Langmuir trough, and a surface pressure (SP) vs mean molecular area (MMA) isotherm was recorded (Figure 3a). The isotherm starts to grow when a MMA value of approximately 250 Å^2 is reached (SP between 0.2-0.5 mN/m), then it reaches a linear regime between SP 10-30 mN/m corresponding to MMA values of approximately 160 Å^2: here the film is homogeneously distributed in 2D (Figure 3c) and there are no segregated clusters that could cause an overestimation in the measured MMA values. A slight flexion at a SP of 30 mN/m is then formed in the isotherm, followed by a more notable one at 60 mN/m; these two values likely corresponding to initial multilayer formation and complete collapse of the film respectively. With MMA values one can already speculate about the packing of **1** at the interface. We chose three specific cases, two of which were often observed in single crystal structures of a parent hydrocarbon molecule[40] and the third one being the desired hexagonal honeycomb-like packing: a) *dense packing*: it involves **1** packing in a dense fashion with a calculated MMA value of 154 Å^2 (Figure S10). Since this model is based on a molecule lacking substituents, this MMA value can be considered as the absolute lowest limit for a monolayer. In fact, in order to sterically accommodate the DEGME chains of **1**, this packing would need to expand a bit resulting in slightly higher MMA values. b) *all-etf packing*: it is based on a model derived from a fragmentary crystal

structure solution of **1** (Figure S7), in which the anthracene units are all in an edge-to-face relationship. For this packing a MMA value of 202 Å² would be expected. c) *all-ftf packing*: it is the desired hexagonal packing ought to provide a 2DP, in which **1** packs with all the anthracene units stacking face-to-face. This last packing has a MMA value of 252 Å² and is based on a theoretical DFT model which will be described in the following paragraph.

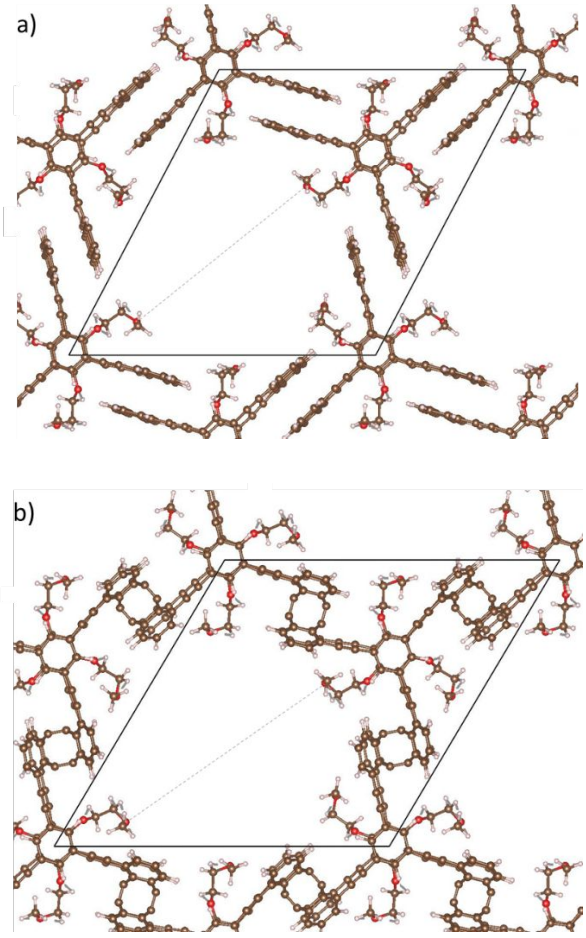

Figure 2. Proposed monomer and polymer packings for monolayers of **1** at the air/water interface obtained from DFT calculations. a) The monomer packing has a hexagonal honeycomb-like structure involving all the anthracene units stacked in a *ftf* relationship; the packing is porous with a pore diameter of 13.5 Å and has a MMA value of 252 Å². b) The polymer packing retains the hexagonal structure and has a pore diameter of 14.3 Å.

To simplify the calculations, we shortened the DEGME chains by three atoms, resulting in ethylene glycol monomethyl ether (EGME) chains (Figure S34). The structure of the monomer was studied in both gas phase and in water solvent in a form of implicit COSMO solvent.[45] The first observation was that the EGME chains in the gas phase, instead of being fully extended, preferred to fold back towards the monomer skeleton in order to maximize the dispersion interactions between anthracenes and chains; more interestingly, the addition of water as solvent even increased this preference (Figure S36). A monomer packing was then assembled, with all the anthracene units being stacked in a *ftf* relationship (Figure 2a). This packing model gives MMA values of 252 Å², which are in perfect agreement with the values observed for an uncompressed self-assembled monolayer (Figure S37). Further, we compared the relative energies of this all-*ftf* with an all-*etf* packing, commonly observed in crystal structures of anthraphanes. In both cases, the ether chains were substituted by hydroxyl groups, to focus only on the effect of the packing (Figure S39). The all-*ftf* packing in the gas phase resulted in a more stable packing by 9.3 kcal/mol per monomer. This energy difference is quite substantial and would justify a preference to form the *ftf* packing at the air/water interface. It is also reasonable to assume that on the surface of water, the anthracene units of the monomer might be partially submerged and experience a hydrophobic effect, thus stacking *ftf* to minimize contact with water. A polymer model obtained from the *ftf* packed monomers was investigated as well and is displayed in Figure 2b). It is interesting to note that both monomer and polymer packings are porous, with a pore diameter of 13.5 Å and 14.3 Å respectively, calculated as the distance between the two closest oxygen atoms across the channels and accounting for vdW radii. This porosity would be particularly interesting for separation applications by using the polymer monolayer as a molecular sieve. As it will be shown in the following sections, spectroscopical data will further strengthen the validity of this packing model. Detailed information on the DFT calculations can be found in the Supplementary Information (Page S37).

The discussion on the correlation between MMA values and packing is valid only if **1** effectively forms monolayers with full coverage between the barriers upon spreading at the air/water interface. We therefore investigated the thickness of the films by tapping mode AFM after transferring them by a modified Langmuir-Schäfer technique on a 285 nm SiO_2-coated silicon substrate. We transferred the films at three relevant features of the isotherm in Figure 1a: without compression at SP of 0.2 mN/m and MMA of 250 Å², in the linear regime at SP of 20 mN/m and MMA of 160 Å², and at SP of 52 mN/m and MMA of 120 Å² (Figure S11). Height profile analysis was performed either at naturally cracked regions of the films or at artificial step edges, created by covering part of the wafers with a piece of freshly cleaved mica before transferring the film. At SP of 0.2 mN/m and 20 mN/m we found thickness values of $h_{AFM} \approx 1.0$ nm, which are in good agreement with the calculated value for the expected monomer orientation at the interface, namely with the long axis of the anthracene units perpendicular to the interface (Figure S12). Other orientations of the monomer on the substrate can be excluded as the expected h_{AFM} would be much higher. The DEGME chains do not seem to contribute to the thickness, meaning that they could either flatten out on the silicon oxide surface or contract back towards the anthracenes, as predicted by the DFT models discussed previously in Figure 2. At SP of 52 mN/m on the other hand, clear double layer formation is observed with $h_{AFM} \approx 2.2$ nm and in some regions high corrugation of the film is present with thicknesses of $h_{AFM} \approx 17$ nm, corresponding to multilayer formation. From the AFM analysis one determines that until the flexion in the isotherm at a SP of 30 mN/m, the monomer films are indeed of monolayer nature and upon further compression multilayers are formed. More interestingly, in the AFM image at 0.2 mN/m one sees that apart from some holes, the monolayer exhibit a certain structural integrity and continuity, hinting at a self-assembly of the monomers at the air/water interface through strong intermolecular

interactions. Visual inspection of the film by Brewster angle microscopy (BAM) showed indeed that upon spreading, the

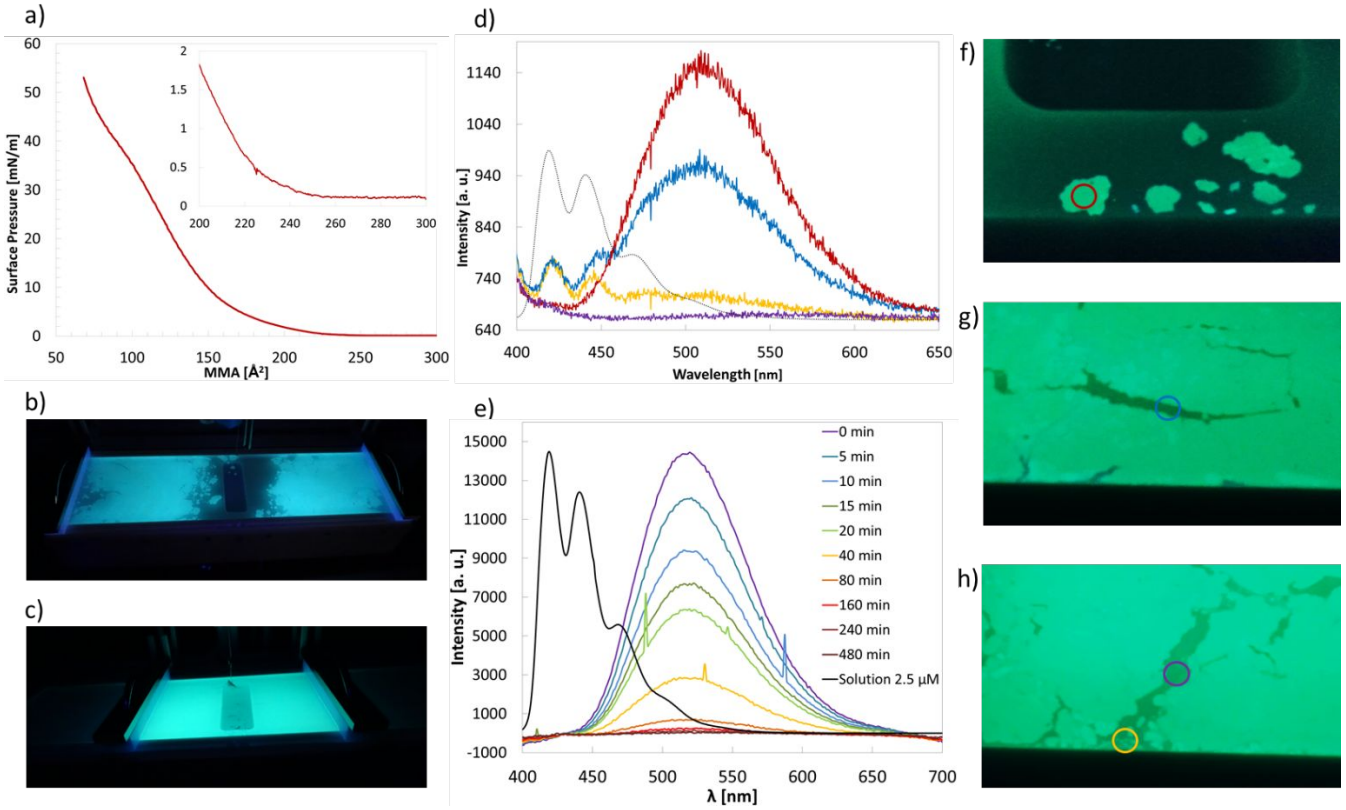

Figure 3. a) SP vs MMA isotherm measured at room temperature after spreading **1** at the air/water interface. In the uncompressed state (0.2 mN/m) the estimated MMA value is 250 Å². b) Freshly spread **1** in a Langmuir trough upon excitation at 254 nm with a UV lamp. c) Same monolayer upon compression to 20 mN/m showing macroscopic homogeneity. d) Fluorescence spectra measured at different areas of the uncompressed monolayer showed in panels f), g) and h); the same color code for the spectra and irradiated areas was retained; a solution spectrum of the monomer is also displayed as comparison as black dotted line. e) *In-situ* fluorescence decay experiment of a monolayer slightly compressed at 0.5 mN/m compared to a solution spectrum of **1** (for excitation and irradiation a wavelength of 365 nm was chosen); the spectra are baseline corrected. f) The fluorescence was measured in the center of a small island marked with a red circle. g) The fluorescence was measured in a crevice of uncompressed monolayer marked with a blue circle. h) The fluorescence was measured between two islands (violet circle) and in a region with a high number of tiny islands (yellow circle).

monomers form islands, which upon compression merge into a homogeneous lateral film with homogeneous thickness, as shown by the monotonous grey contrast on the micrographs (Figure S13).

From the packing considerations exposed previously and the AFM analysis we concluded that upon spreading the monomer self-assembles into a packing with MMA values of 250 Å², in good agreement with the desired all-*ftf* packing model; it then reaches upon compression a linear regime between 10-30 mN/m with a MMA of 160 Å², corresponding to the densest achievable packing for the monolayer, which upon further compression collapses into a multilayered film.

Photochemical environment at the air/water interface. A characteristic of anthraphane compounds is their intense fluorescence (both in solution and solid/crystalline state) and we discovered that this characteristic is retained in monolayers of **1**, which exhibit striking blue-green fluorescence when excited with a standard UV lamp at 254 nm. The monolayers can in fact be visualized by naked eye with great detail, providing a "bird's eye view" with respect to BAM images and with enough detail to distinguish islands formation and homogeneity (Figure 3b-c and Figure S14). This intense fluorescence is so far exclusive to **1** since it was not observed with other anthracene-based monomers used at the air/water interface.[15,16,18,19] We exploited this phenomenon to record a movie of the spreading process which can be found as Supplementary Information. In the footage, one sees the typical deep blue fluorescence of the solution of **1** in the syringe cylinder and hanging as a droplet on the tip of the needle; when the droplet touches and spread on the surface of the water, small islands with blue-green fluorescence are immediately formed, which over time and upon solvent evaporation coalesce into larger islands. It can be noted in particular that the shape of the islands and more in general the edges of the monolayer have very well-defined and sharp features, compared to the line tension-governed circular shapes that one observes for instance with oil droplets floating on the surface of water. The formation of the sharp edges could therefore be a hint of crystallization of **1** taking place on the surface of water through particularly strong anthracene-

anthracene interactions. Another important observation is that upon compression of the monolayers, fluorescence is not observed outside the barriers of the Langmuir trough, excluding diffusion of the monomer in the subphase.

For a 2D-polymerization to take place, it is necessary that in the monolayer all the anthracene units of **1** are *ftf*-stacked, so that upon excitation, excimers are formed which can then decay into an anthracene dimer upon [4+4]-cycloadditon. Excimer emission is very characteristic, being broad, unstructured and considerably red-shifted with respect to the typical vibronic signature emission of free unpaired anthracene units.[46] We therefore investigated the photochemical environment of the monolayer at the interface by *in-situ* fluorescence spectroscopy. According to the UV/Vis absorption spectrum of the monomer monolayer on quartz (Figure S15) a wavelength of 365 nm was selected for excitation. The first measurement was performed on an uncompressed large and continuous monolayer region by focusing the excitation LED to a circular spot of about 5 mm in diameter and measuring the fluorescence response with a read-out fiber connected to a spectrometer as shown in Figure S16. Delightfully, a pure excimer fluorescence was observed with a typical unstructured broad spectrum centered at around 510 nm; no sign of the vibronic structure of isolated anthracenes could be detected. Absence of vibronic splitting may have another reason *i.e.* the chance for energy transfer from unpaired anthracenes to paired ones which will be dealt with in the following section. We then exploited the fact that the monolayers can be visualized by naked eye to measure the fluorescence in specific areas with specific features of an uncompressed monolayer (Figure 3d). We first focused the excitation beam in the center of a 1 cm-sized island (Figure 3f) and we surprisingly obtained again a pure excimer emission.

This packing model would imply that at edges of a monolayer, free unpaired anthracene must be present acting as edge groups. We therefore measured the emission at a crevice in the monolayer, encompassing with the excitation beam both the edges and internal regions (Figure 3g). Gratifyingly, what resulted from this measurement is a mixed state of usual excimer emission and a new emission with vibronic features typical for isolated anthracenes, which is virtually superimposable with the emission spectrum of **1** in solution (black dotted spectrum in Figure 3d). From the blue spectrum in Figure 2d one can qualitatively see that at the measured area the concentration of paired anthracene is much larger than the free anthracenes at the edges. We therefore moved to an area of the monolayer with a particular high concentration of microscopic island with fractal edges (Figure 3h, yellow circle): in this area we expected a higher concentration of free anthracenes with respect to paired anthracene and this was confirmed by the emission spectrum (yellow in Figure 3d). Finally, we measured the fluorescence between two islands (Figure 3h, purple circle) and we obtained virtually no fluorescence response in the sensitivity level of the measurement: this experiment suggests that there is no appreciable diffusion of monomers between islands and more in general that there are no free floating monomers in non-covered regions.

Photochemical 2D-polymerization reaction. We next turned our attention to the potential 2D-polymerization reaction, namely if all the excimer pairs in the monolayer can efficiently be converted into anthracene dimers, creating net-points and resulting in a free-standing covalently bound monolayer. An *in-situ* fluorescence decay experiment was therefore conducted by monitoring the decay of the excimer population during the irradiation time. The irradiation was performed at ambient conditions, by using 365 nm fiber-coupled LED (250 mW) as irradiation and excitation wavelength. The results are summarized in Figure 3e. After approximately 4 h, no residual intensity from the excimer emission was visible, indicating that the excited pairs were consumed. The decay of the excimers followed well-behaved first order kinetics (Figure S17) with no changes in the shape of the excimer peaks, indicating that the phenomenon behind intensity decay does not change its nature. More importantly, as the population of excimers decayed, no emission from unpaired anthracenes developed, reinforcing the idea of having an all *ftf*-packing. A possible reason for the absence of fluorescence of unpaired anthracenes could be due to energy transfer, but the fact that vibronic splitting can be detected at the edges of the monolayer shows that energy transfer cannot disguise unpaired anthracenes. Another possible reason could be due to the oxidation of free anthracenes with atmospheric oxygen: endoperoxide formation by photooxidation of anthracenes with consequent formation of anthraquinones is a well-known phenomenon.[47–51] Endoperoxide formation would simply destroy the anthracene units, rendering them unable to contribute to the formation of net points. If this reaction would be significantly competitive with the anthracene dimerisation, considerable defects would be formed in the molecular network, having detrimental effects for its mechanical stability. This point will be addressed below.

While providing important information, fluorescence spectroscopy only shows that the excimer pairs are consumed but it does not give any information about the eventual formation of bonds between anthracenes. To address this issue we performed TERS on irradiated monolayers after transferring them onto template stripped gold substrates. In order to irradiate large areas, a custom-made 385 nm LED (1 W) was used (Figure S18). After 2 h of irradiation, peaks at 1385 cm^{-1} and 1560 cm^{-1} corresponding to typical anthracene vibration modes decrease, while a new peak at 1600 cm^{-1} corresponding to the anthracene dimer appears (Figure S19).[15,21] The peak corresponding to the triple bonds at 2214 cm^{-1} also seems to get weaker after irradiation; the intensity of this signal is however very sensitive to the spatial orientation of the triple bonds with respect to the substrate and can vary greatly from sample to sample. Crystal structures of anthraphanes[40] show that the acetylenic units of the monomers are indeed quite flexible; as such, conformational readjustments of the polymeric structure might be the cause of the different intensities observed. The peak at 995 cm^{-1}, which corresponds to the breathing mode of the benzene moiety of the monomer and is not affected by the photoreaction, was chosen as reference to estimate the conversion of the polymerization. By calculating the ratio between the anthracene peak at 1385 cm^{-1} and the one at 995 cm^{-1}, a conversion of 82.4% was estimated. These results are in good agreement with the fluorescence decay experiment illustrated previously and show that very high polymerization conversions can be achieved. Moreover in the TERS spectra there is no appreciable sign of peaks at 1750 cm^{-1}, which would correspond to the carbonyl groups of anthraquinones formed

by anthracene photooxidation. As such, the role of oxygen during photoirradiation can be considered as negligible.

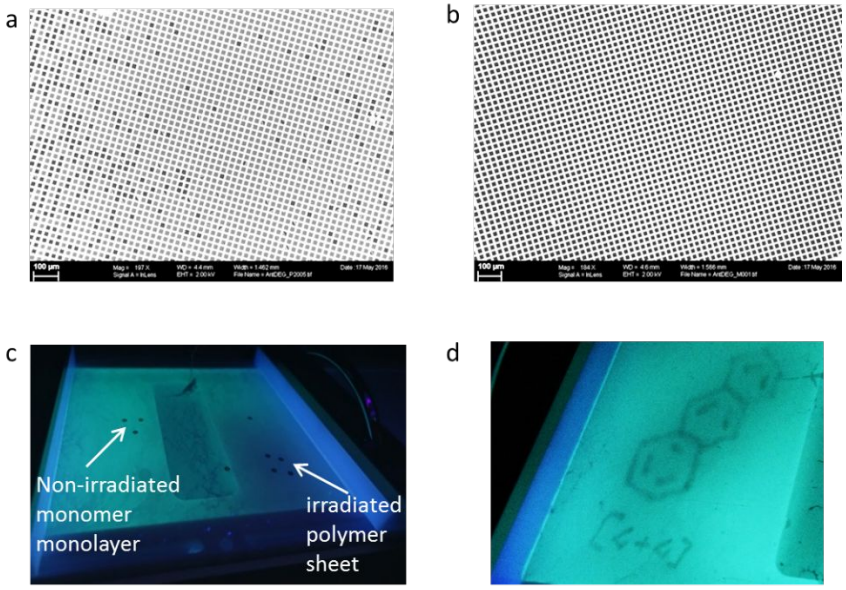

Figure 4. a) SEM images of irradiated monolayer transferred onto TEM grids spanning holes of 20 μm × 20 μm; polymerization converts the anthracene pairs into net points (anthracene dimers) which confer mechanical integrity to the polymer. b) Control experiment of non-irradiated monolayer transferred onto TEM grids: the holes are not spanned since there is no mechanical integrity in the monomer monolayer. c) After polymerization, the irradiated areas are completely bleached; the irradiated (polymer) and non-irradiated (monomer) areas are transferred on copper TEM grids for SEM analysis (the grids appear as black circles in the image). d) Writing on a monomer monolayer directly at the air/water interface using a 405 nm laser pointer: in this case an anthracene molecule was drawn with a "[4+4]" text, referring to the type of cycloaddition reaction responsible for the polymerization.

As expected, the polymerization reaction also found direct visual confirmation since the irradiated areas are bleached due to complete consumption of the excimer pairs (Figure 4c). To have a more tangible confirmation of the conversion values obtained by TERS, we qualitatively investigated the mechanical integrity of the polymer sheet. A self-sustaining network is expected to span the holes without collapsing under its own weight, while the molecules in the monomer monolayer, lacking in-plane bond formation, are expected to simply pass through the holes. SEM analysis confirmed this assumption as can be seen in Figure 4a-b: the polymer film spanned efficiently over the 20 μm × 20 μm holes, with occasional ruptures attributed to the transfer procedure, while in the monomer case, no hole could be spanned.

This experiment supports that irradiation and subsequent anthracene dimerisation is the cause of the observed mechanical stability. For a hexagonal 6^3 honeycomb lattice,[52] which suits our packing model in which all the anthracene units of **1** are *ftf*-paired, the bond percolation threshold is 65%. The conversion values obtained by TERS are way above this value and reflect the mechanical coherence observed by SEM. As discussed before, anthracene photooxidation cannot be completely excluded, but formation of anthracene peroxides (which subsequently decay into anthraquinones) would involve formation of defects in the network, which would impact negatively its mechanical stability. As such, it can be concluded that photooxidation is not a major competitive reaction to the anthracene dimerisation. This conclusion was also reinforced by XPS analysis (Figure S20), which was initially performed to also estimate the conversion of the polymerization reaction by comparing the ratio between the sp^2 aromatic carbons and the newly formed sp^3 carbon atoms of the dianthracene bridges. Unfortunately, the chemical shifts of these atoms were too small and impeded a reliable distinction from the data fits. Nevertheless, the ratio between the total oxygen to carbon concentration could be obtained from the integrated intensities of the O1s and C1s peaks and resulted constant for irradiation times up to 2 h.

Overall, the combined results of the isotherm measurements, fluorescence spectroscopy, TERS analysis and SEM analysis, further strengthen our hypothesis of having an all-*ftf* packing as the one proposed in our DFT models. To briefly summarize: when applied at the air/water interface, **1** self-assembles into monolayer islands which have a characteristic excimer emission, indicating a face-to-face stacking interaction between the anthracene units; no sign of isolated unpaired anthracene can be found, except at the edges of the islands. Upon compression, the surface pressure starts to rise when a MMA value of around 250 $Å^2$ is reached. Upon photoirradiation, the excimer fluorescence virtually decays to zero and according to TERS, the vibrational modes typical for anthracenes decrease, while new vibrational modes corresponding to the anthracene dimer motif appear. By transferring the irradiated monolayer on a holey support, SEM reveals that the monolayer is free-standing.

Patterned Photolitography with Photoreactive Monolayers. Having performed the photopolymerization *in-situ* at the air/water interface and spectroscopically ascertained the chemical nature of the obtained polymer

monolayer, we started to investigate the possibility of using monomer monolayers of **1** as recyclable molecular paper. Their high fluorescence can be quenched by the 2D-polymerization reaction, resulting in non-fluorescent polymerized areas and still fluorescent monomeric areas (Figure 4c). The idea behind a recyclable molecular paper is that one can freely draw (bleach) on the monolayer, erase the writing by recovering the fluorescence back, and rewrite on the monolayer. The recovery of the fluorescence would be possible by the intrinsic thermal reversibility of [4+4]-cycloadditions. In a previous study, dimers of the hydrocarbon anthraphane were found to revert back to the monomers starting at 180°C, whereas linear polymers had higher thermal stability, reverting back to monomers starting at 200°C.[39,41] We first performed the writing/bleaching by using a 200 mW violet laser pointer (405 nm) directly at the air/water interface: the results were particularly suggestive as the bleaching occurred in seconds and by using a laser pointer patterns could be drawn as desired (Figure 4d). The patterned monolayer could then be easily transferred on a PET film (mylar) by simply depositing the film on the water surface on the bleached area (Figure S22). In order to test the thermal reversibility of the [4+4]-cycloaddition, we transferred the monolayers on a 285 nm SiO_2-coated silicon substrates and performed the bleaching in a more controlled environment of a confocal laser scanning microscope (CLSM). We first checked the emission of the monomer monolayer on the substrate and an excimer signal centered at around 513 nm was detected (Figure S25): this is an indication that the transfer process from the water surface to the substrate does not affect the molecular packing (fully comparable with a monolayer transferred on quartz in Figure S15). We then bleached a star pattern on the monolayer by using the 405 nm laser of the confocal microscope, observing in the polymerized area a drop of the fluorescence by 90% (Figure S23-S25). We then heated the wafer at 200°C for 4 h under nitrogen and checked the fluorescence again by using the same detector settings as before: unfortunately, the heating process considerably degraded the entire monolayer, dropping the overall fluorescence intensity by 90% of its original value (Figure S26-S27). By increasing the detector sensitivity the star pattern was nevertheless still present. We tried different temperatures ranging from 180 to 235°C and different heating times ranging from 2-24 h, but in all cases the degradation of the monolayer was observed. Only in one instance we were able to successfully perform a bleaching-regeneration-bleaching cycle by heating the substrate to 200°C for 2 h and then at 235°C for 4 h (Figure S28). While this process was scarcely reproducible and again accompanied by a drastic decrease in the fluorescence intensity, this is the first example of a successful optically-rewritable molecular paper exploiting 2D-polymerizations. In another study with a different molecule, the fluorescence could be recovered after bleaching, but it was not possible to rewrite on the regenerated areas; information on the fluorescence intensities before and after the heating process were unfortunately not reported.[27] In the case of **1**, it seems that the anthracene dimer motif is thermally too stable and that there is a competition between the depolymerization reaction and the degradation of the monolayer. To avoid this problem, we anticipate that **1** could be modified to bear substituted 1,8-diazaanthracenes, whose dimers have proven to thermally revert already at 120°C in solution.[53,54] As a control experiment for the overall stability of the monomer monolayers, we compared the fluorescence intensity of a freshly prepared monolayer and the same sample after being stored in a drawer for 5 days: we observed an overall drop in the fluorescence intensity by approximately 10% (Figure S29), we cannot however completely exclude that this drop might be due to accidental light exposure during sample preparation and transportation to the fluorescence microscope.

Due to the limited applications of the monolayers of **1** as molecular paper, we turned our attention to their possible use in lithographic processes. In particular, the idea was to exploit the difference in solubility and adhesion to the substrate between monomer and polymer, and effectively use the monomer monolayer as a negative photoresist. We prepared a 1.5 x 1.5 cm sized square 285 nm SiO_2-coated silicon wafer with a small piece of mica covering its corner and transferred a monolayer onto it; the mica was then removed in order to have a well-defined monolayer-free area as control region (Figure 5a).

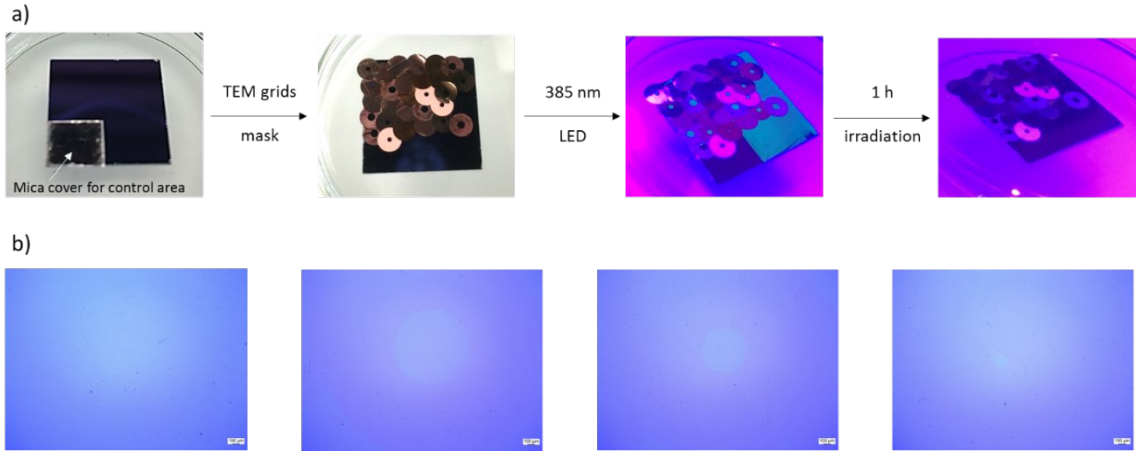

Figure 5. Photolithography using a 2D-polymerization in monolayers. a) In a simple process monolayers of **1** are transferred on a silicon oxide wafer (a mica slide is placed on the wafer prior to transfer in order to have non-covered part as control region); single-hole TEM grids are applied as masks on the wafer, which is then irradiated with a 385 nm LED; the monolayer-covered areas gradually lose their fluorescence as the polymerization reaction proceeds. b) Optical micrographs in differential interference contrast; from *left* to *right*: micrograph of the wafer after the irradiation showing a homogeneous blue color corresponding to a monolayer-covered area; wafers after washing with chloroform and isopropanol showing the lithographically imprinted circular

monolayer with diameters of 1000 μm, 600 μm, and 200 μm, corresponding to the diameters of the single-hole TEM grids used as mask. The bare silicon oxide surface appears violet in color whereas the monolayer-covered regions are sky blue (scale bars are 100 μm).

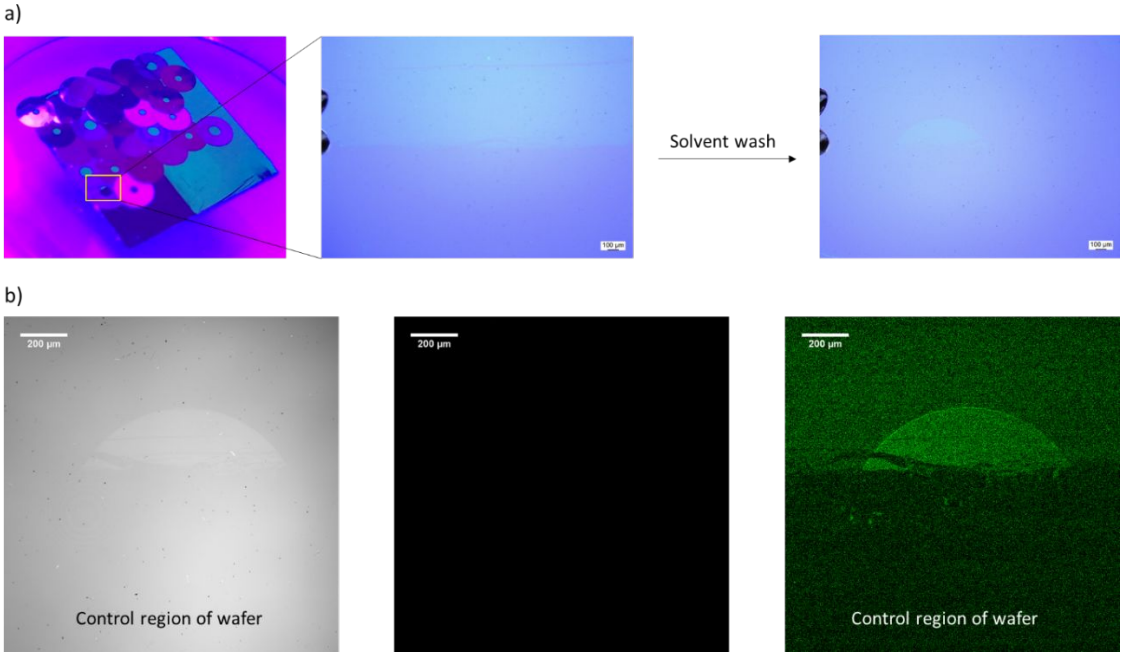

Figure 6. Photolithography at the boundary of the control region. a) A single-hole TEM grid was placed at the boundary between monolayer-covered and non-covered wafer; after the lithographic process a monolayer shaped as a circular segment was created (scale bars are 100 μm). b) The monolayer circular segment was identified under the confocal fluorescence microscope in reflection mode (*left*) and the emission was recorded; no fluorescence was observed by using the same detector settings for a fresh monolayer (*center*), indicating that the unreacted monomers were successfully washed away from the substrate; by increasing the detector sensitivity the control region starts to emit as noise: the difference in intensities between control, irradiated, and washed regions is minimal *(right)*.

We then checked the wafer under an optical microscope in differential interference contrast (DIC) and observed a clear difference in contrast between monolayer-covered regions which appeared sky blue and bare silicon oxide which appeared violet in color (Figure S30). The boundaries of the control region could be easily identified as well as some natural cracks in the monolayer occurred due to the transfer process. We then covered part of the wafer with single-hole TEM grids with different hole diameter (100 μm, 200 μm, 600 μm and 1000 μm) as mask and proceeded to irradiate the wafer with a 385 nm LED (1 W). As can be seen in Figure 5a, the monolayer-covered areas are highly green fluorescent, whereas the control area does not emit. When the fluorescence completely disappeared after 1 h of irradiation, we again checked the wafer under the optical microscope and assessed no difference in contrast nor coloration between polymerized and non-polymerized monolayer (Figure S31). We then immersed the wafer in a chloroform solution for 1 min, and slowly pulled it out by constantly rinsing it with isopropanol in order to remove any residual chloroform from its surface. This step is crucial because by leaving the chloroform to evaporate on the wafer it will cover it with impurities; the isopropanol was then quickly blown away with an air gun leaving the dried substrate. Analysis under the microscope gratifyingly showed that the irradiated areas stayed on the wafer while the non-irradiated parts were completely washed away, leaving circular-shaped monolayers with diameters corresponding to the diameters of the employed masks (Figure 5b and Figure S32).

To check the efficiency of the irradiation and washing process, we strategically placed a single-hole TEM grid at the boundary of the control zone, encompassing both monolayer-covered and non-covered areas (Figure 6a). After the lithographic process, a monolayer shaped as a circular segment was left on the silicon oxide wafer. We searched the same feature under the confocal fluorescence microscope and measured the fluorescence intensity by using the detector settings used for a fresh non-irradiated monolayer (Figure 5b) and gratifyingly no fluorescence could be detected. The detector sensitivity was increased until the control region also started to emit as noise: under these settings, the difference in intensities between the control region and the previously covered region was minimal, indicating that the unreacted monomer was indeed efficiently washed away from the substrate. The irradiated area also appeared slightly fluorescent but these could be due to the relatively short irradiation time employed (figure S33). Overall one can conclude that the lithographic process using masks is efficient.

Next we focused our attention on the possibility of performing the lithography at a smaller scale and with freely drawn shapes, without using masks. To do this we exploited the confocal laser scanning microscope: we prepared a wafer covered with a monolayer and visualized it in phase contrast

mode using the laser at 633 nm, so that upon scanning, no light that would trigger unwanted polymerizations was absorbed by the monolayer. We then selected three regions on the monolayer in the shape of a square, circle and triangle inside of which the 405 nm laser was selectively activated

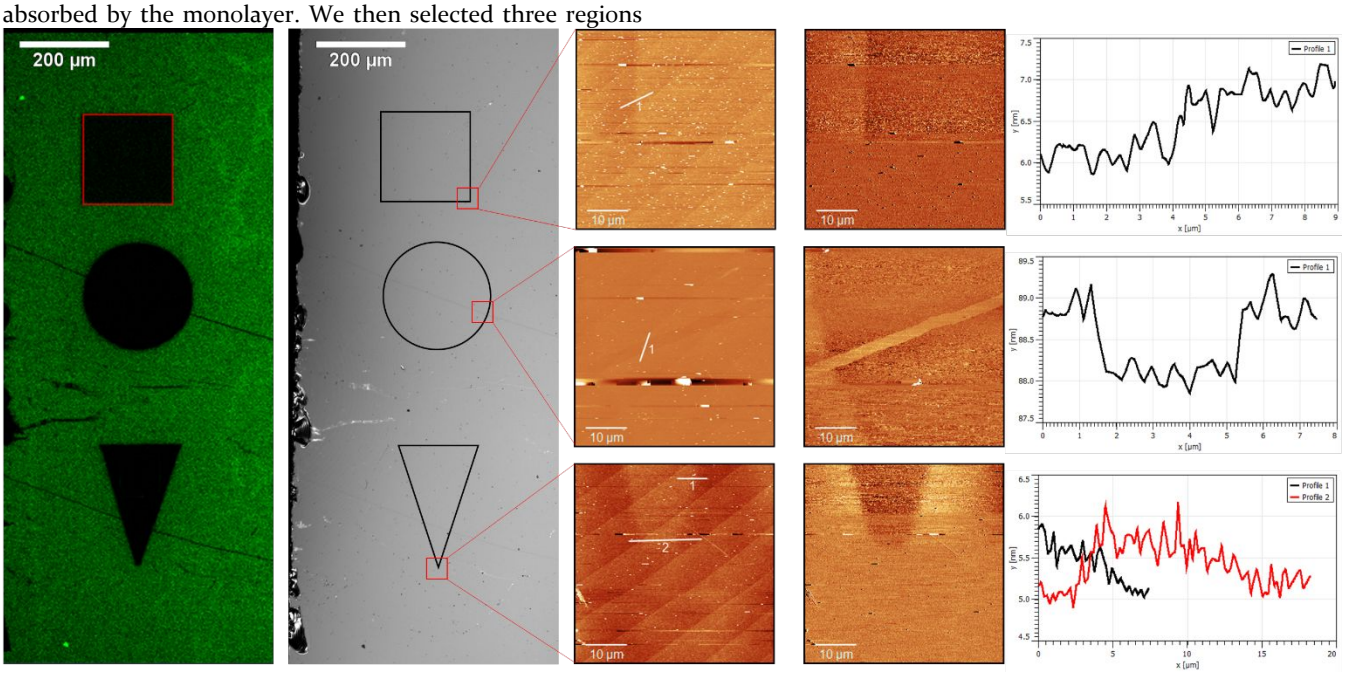

Figure 7. Photolithography in monolayers at the microscopic level with a confocal scanning laser microscope. A monolayer of **1** is deposited on a silicon oxide wafer and imaged with the confocal laser microscope: in the left micrograph the monolayer is scanned with a 405 nm laser, displaying the typical green excimer fluorescence. To avoid unwanted polymerization during the scanning process, a 633 nm laser can also be used as shown in the second micrograph: the monolayer is nevertheless visible due to the phase contrast. Regions are then defined inside of which the polymerizing 405 nm laser is turned on, in this case a square, a circle and a triangle, marked as black lines in the figure. After the irradiation the wafer is washed and imaged by AFM where the lithographically imprinted shapes are visible both in the height and phase imaging. In this case a corner of the square, the edge of the circle and the tip of the triangle are visible. In the circular shape, a natural crack of the monolayer is clearly visible. Height profiles at different edges confirm the monolayer nature of these macromolecular 2D objects. The optical micrograph is mirrored with respect to the AFM images because the substrate is mounted upside-down in the confocal laser microscope.

while scanning with the 633 nm laser. We performed the usual washing procedure of the wafer and then tried to visualize the lithographically imprinted shapes by AFM. While the substrate appeared slightly dirty, we could nevertheless obtain some images featuring a corner of the square, the border of the circle with a natural crack propagating inside the shape, and the tip of the triangle, as seen in Figure 7. While in the height images it was somewhat difficult to find the imprinted shapes, in the phase images the outlines were much clearer. Height analysis confirmed the shapes to be monolayer molecular objects with $h_{AFM} \approx 0.8$-0.9 nm. The step edges were found to be more clear-cut in some regions than others: we believe that this might be due to the washing process, which might leave some contaminations on the silicon oxide surface, rendering the visualization of the step edges less clear.

With these experiments we demonstrate that it is possible to use 2D-polymerizations in molecular monolayers as a lithographic process for producing arbitrarily shaped 1 nm thick two-dimensional macromolecular objects.

CONCLUSIONS

In conclusion we have synthesized an amphiphilic trifunctional photoreactive monomer, the anthraphane-tri(DEGME) **1**, which upon spreading at the air/water interface forms highly fluorescent self-assembled 1 nm-thick monolayers. The monolayers are suggestively visible by naked eye upon excitation with a UV lamp. A thorough *in-situ* fluorescence spectroscopy study, reveals that self-assembly occurs by π-π stacking between the anthracene units of the monomers, resulting in monolayers with pure excimeric emission at 510 nm, while at the edges of the monolayer, free isolated anthracenes are present. Photoirradiation of the monolayers results in a 2D-polymerization *via* dimerization of the stacked anthracene pairs through [4+4]-cycloaddition and the polymerized monolayers are free-standing when spanned over microscopic holes. In the irradiated/polymerized areas of the monolayer, the fluorescence is completely quenched resulting in a clear differences in contrast. These characteristics are fully retained when the monolayers are transferred on solid substrates. By using a 405 nm laser it is possible to freely draw and imprint patterns on the monolayers suggesting their use as molecular paper. More importantly, we have developed a lithographic process which allows to create 1 nm-thin 2D monolayered objects in the desired lateral size and shape, both by using masking techniques and the guided laser of a confocal fluorescence microscope. The monolayer acts as a negative photoresist and the non-irradiated monomeric areas can be removed by simple solvent washing, leaving the desired 2D macromolecular shape. Being the polymer an electrical insulator, it would be possible for instance to create insulating

monolayers in arbitrary sizes and shapes. The free anthracenes at the edges of the polymer would also be available for further functionalization.[55] This study not only shows that it is possible to use 2D polymerizations for lithographic processes, but it also has some more fundamental implications such as the possibility of controlling the molar mass of the polymers: by exploiting the step-growth polymerization mechanism areas of different size are irradiated, resulting in polymers with molar masses depending on the irradiated area only. While this process has a large error bar due to the limitations associated with the spatial resolution of light, it is controlled in the sense that each anthracene pair responds to the excitation with a yes/no answer and therefore unintended polymerizations are not present in non-irradiated areas. This work opens the possibility of synthesizing macromolecules by light-directed nanosynthesis[56] and it could also be the basis for pointing towards the relation between selected-area photochemical synthesis (SAPS) in crystalline monolayers and common concepts of organic chemistry such as structural isomerism and stereochemistry, by for instance creating specular 2D objects. While currently these concepts may appear a bit far-fetched, the simple experiments provided in this study could support this view in the future.

METHODS

Synthesis of amphiphilic monomer 1. Precursor **6** (500 mg, 0.44 mmol, 1.00 eq) was suspended in 222 mL dry toluene (2.00 mM) with compound **5** (225 mg, 0.44 mmol, 1.00 eq) and dry triethylamine (12.4 mL, 89.0 mmol, 200 eq). The reaction mixture was degassed by cooling it to -80°C with an acetone-dry ice bath and then performing five cycles of vacuum (10 min) and nitrogen backfilling. $Pd(PPh_3)_4$ (154 mg, 0.13 mmol, 0.30 eq) was added with N_2 counter-flow and the suspension was degassed twice again and backfilled with argon after the last cycle. After warming to room temperature, the reaction mixture was put in a preheated bath at 80°C and stirred in the dark under argon for 5 d. After cooling to room temperature, the reaction mixture was filtered and the filtrate was concentrated to dryness. The brownish residue was washed with MeOH to obtain a beige solid, which was collected by filtration and rinsed with more MeOH until the filtrate resulted colorless. The crude product was then purified by column chromatography (1% MeOH in DCM) and the obtained solid was recrystallized from boiling THF to obtain **2b** as pale yellow needles (217 mg, 0.16 mmol, 42%). Compounds characterizations and additional details on the synthetic sequences to compound **5** and **6** can be found in the Supporting Information.

Preparation of self-assembled monolayers of 1. A KSV 2000 System 2 Langmuir trough equipped with a platinum Wilhelmy plate and dipper was used for this study. The trough was made of Teflon® and the barriers were of hydrophilic Delrin®. As subphase, Millipore water was used. For the cleaning procedure, the trough was first rinsed with Millipore water followed by chloroform, ethanol and chloroform again by wiping it with dust-free paper to remove all traces of organic material. The barriers were cleaned and wiped with ethanol and Millipore water. The trough was then filled with Millipore water and its surface treated by vacuum-suction to remove residual particles of dirt (cleanliness of the water surface was checked by UV lamp for residual fluorescence and by Brewster's angle microscopy). The Wilhelmy plate was rinsed with water and ethanol and then heated for a few seconds on a burner to incandescence. For spreading of **1**, a stock solution (0.25 mg/mL) of a 1:1 solvent mixture of chloroform/cyclohexane was prepared. The solution was spread dropwise at the interface with the use of an air-tight glass microsyringe. Typical applied volumes were 200 µL. The solution was stored in a glass vial in the dark. After spreading, 30 min were waited to allow complete evaporation of the solvents..

Transfer of the monolayers on substrates. The monolayers were transferred horizontally at constant surface pressure using a modified Langmuir-Schaefer-technique (Figure S9): a tilted stage with the substrate was attached to the dipper and immersed just below the water surface; after spreading and reaching the target surface pressure, the stage was slowly pulled out of the water (transfer rate 0.5 mm/min) and the substrate left to dry overnight. The substrates used were: silicon oxide (285 nm) on silicon for AFM, template stripped gold for TERS and gold on silicon oxide for XPS.

AFM analysis of the monolayers. Height analysis was performed by using a Nanoscope III Multimode system (Digital Instruments, Santa Barbara, Ca). OMCLAC160TS silicon tips (Olympus, Tokyo, Japan) were used for imaging with a resonance frequency in between 200 and 400 kHz and a spring constant of about 42 N/m. The Langmuir films were transferred horizontally on 285 nm SiO_2-coated silicon wafers.

Brewster's angle microscopy. To visualize the films by Brewster angle microscopy (BAM), a KSV MicroBAM operating by a 659 nm laser was used.

Fluorescence of the monolayers at the air/water interface. To visualize the monolayers by naked eye, a standard portable laboratory UV lamp for TLC (Camag) was used at 254 nm. For recording the fluorescence spectra at the interface, an Acton series spectrometer from Princeton Instruments (NJ, USA) was used. The spectrometer was equipped with an SP-2556 Acton Research 500 mm Imaging Spectrograph (Acton, MA, USA), FC fiber stage (modified in house to be 3 mm closer to the reflecting mirror) and three standard gratings with groove densities of 1200 mm^{-1}, 600 mm^{-1} and 150 mm^{-1}, with blaze size of 500 nm and 68 mm x 68 mm dimensional size. The CCD camera mounted on the spectrograph was a Princeton Instruments PIXIS 256E (NJ, USA). The read-out fiber was purchased from AFW Technologies Pty Ltd (Hallam, Australia) and had a core diameter of 50 µm, numerical aperture of 0.12 and FC connectors on both ends. The light source used for excitation of the monomers on the interface was an LED with λ = 365 nm and with 250 mW power (Omicron Laser, Rodgau, Germany). It was mounted on a lens tube along with a UV fused silica bi-convex lens with 40 mm focal length (Thorlabs, LB4030-UV, Newton, NJ, USA) as well as a band-pass filter transmitting at 370 nm with FWHM of 10 nm (Thorlabs, FB370-10, Newton, NJ, USA). The beam was focused at the interface to produce an illuminating spot with a diameter of about 2 mm. The read-out fiber was aligned and focused to maximize the emission signal. The exposure time for simple measurements was 30 seconds whereas for the fluorescence decay experiment it was 60 seconds for each spectrum while the LED was at full power during the acquisition time. The delay time between the spectra was 2 minutes. A binning of 4 was used to record the data. The CCD read-out was set to the region of interest (ROI), while the ROI set-up on the slit ran from 130 as the start point with a height of 23. During the course of the fluorescence

decay experiment the entire set-up (LED for excitation and detector for collecting the fluorescence emission) was kept in a fixed geometry. The set-up for the experiment is shown in Figure S16.

Polymerization at the air/water interface. The monomer monolayers were polymerized by direct exposure to a custom-made 385 nm LED with 1 W of nominal power (Figure S18). The irradiation areas could be varied by varying the distance of the LED from the interface.

Tip-enhanced Raman spectroscopy. STM-TERS measurements were performed on a top illumination TERS instrument that combines STM with a Raman spectrometer (NT-MDT, Russia, NTEGRA Spectra Upright). An electrochemically etched Ag tip was used to obtain both the topography and TER spectra. The 632.8 nm He-Ne laser was used as an excitation source. For all the measurements, the tunneling conditions were 200 pA and 0.2 V, the intensity of laser was 30 μW with 1 s exposure time. As substrate, template stripped gold was used.

Scanning electron microscopy. TEM copper grids with the mesh size of 1000 (PLANO, G2780C) were placed on the irradiated spot on the surface of the water. A clean white piece of paper was then gently put on the grids so for them to adsorb on it. The paper along with the grids on it was then removed by hand and dried overnight at room temperature. The TEM grids were placed on a PLANO G3662 holder and imaged with FEG-SEM, Zeiss LEO Gemini 1530, Germany, microscope with an in-lens detector.

X-ray photoelectron spectroscopy. A Quantum 2000 (Physical Electronics Inc.) instrument under ultrahigh vacuum (<5 × 10−7 Pa) was used. Monochromatic Al Kα X-rays with a photon energy hν = 1486.7 eV were used, and the data were recorded at an analyzer pass energy of 23.50 eV and a step size of 0.1 eV (for the detailed spectra) and a pass energy of 58.70 eV and a step size of 0.5 eV for the survey. Argon ions and electron neutralizers were used to compensate for surface charging.

Confocal laser scanning microscopy. A Zeiss LSM 780 laser scanning confocal microscope (Oberkochen, Germany) was used. The system was equipped with a motorized X-Y stage (135 cm × 80 cm) and two conventional PMTs and a highly sensitive, multiarray 32PMT GaAsP detector for fast spectral scanning. Images were recorded using a laser line of 405 nm (diode) and a 10X, 0.3NA EC Plan-Neofluar Ph1 M27 objective. Lambda scans were conducted using a laser line of 405 nm, a filter of 446-695 nm and a lambda window distance of 8.9 nm. Data processing was carried out using the ZEN Black 2012 software by Zeiss (Oberkochen, Germany) and Fiji (U.S. National Institutes of Health, Bethesda, Maryland, USA). Contrast and/or Brightness of images were increased to obtain optimal image quality. The monolayers were transferred on 285 nm SiO_2-coated silicon wafers.

Photolithography procedure. The monomer monolayer was transferred on a 1.5 x 1.5 cm sized square 285 nm SiO_2-coated silicon wafer. Masks were then applied on the substrate, followed by irradiation with a 385 nm LED (1 W) for 1 h. The wafer was then immersed in a chloroform solution for 1 min to remove the non-irradiated parts. Afterwards it was slowly pulled out with tweezers under a constant rinsing with isopropanol in order to remove any residual chloroform from its surface. The isopropanol was then quickly blown away with an air gun leaving the dried substrate with only the photopolymerized regions on it. Alternatively, instead of using masks, desired patterns can be freely photopolymerized on the substrate by using the laser (405 nm) of a confocal scanning microscope.

Molecular models. Calculations were performed in the ADF modeling suite using density functional theory (DFT) methods; the cluster model calculations were done in the program ADF and periodic model calculations in BAND. The functional PBE was used in all calculations together with the D3 empirical dispersion correction with Becke-Johnson damping. The TZP basis set was utilized for all cluster model calculations and DZP for calculations with periodic structures. For additional details, see Supporting Information page S37.

ASSOCIATED CONTENT

Supporting Information. Synthesis and characterization of the monomer, video of the spreading process, isotherms and AFM analysis of the monolayers, BAM micrographs, UV/Vis absorption and emission spectra, TERS spectra, XPS data, confocal laser microscope data, optical micrographs, DFT calculations.
This material is available free of charge *via* the Internet at http://pubs.acs.org.

AUTHOR INFORMATION

Corresponding Author

*E-mail: marcosendymion@gmail.com

ACKNOWLEDGMENTS

The authors would like to thank Prof. J. Vermant (ETH Zurich) for providing access to light microscope and Prof. A. Studart for access to SEM. Many thanks go to Prof. N. Spencer (ETH Zurich) for providing access to AFM and to Dr. W. Dai for helping with the preparation of the gold substrates for XPS and silicon oxide substrates for AFM measurements. The help of Dr. Gabriele Fenini (Zurich University Hospital) with the photos of the fluorescent Langmuir monolayers is greatly appreciated. The authors acknowledge support of the Scientific Center for Optical and Electron Microscopy ScopeM of the Swiss Federal Institute of Technology ETHZ. ZIH Dresden is thanked for computational resources.

REFERENCES

(1) Sakamoto, J.; Van Heijst, J.; Lukin, O.; Schlüter, A. D. Two-Dimensional Polymers: Just a Dream of Synthetic Chemists? *Angew. Chem. Int. Ed.* **2009**, *48*, 1030–1069.

(2) Servalli, M.; Schlüter, A. D. Synthetic Two-Dimensional Polymers. *Annu. Rev. Mat. Res.* **2017**, *47*, 361-389.

(3) Colson, J. W.; Dichtel, W. R. Rationally Synthesized Two-Dimensional Polymers. *Nat. Chem.* **2013**, *5*, 453–465.

(4) Servalli, M.; Öttinger, H. C.; Schlüter, A. D. Synthesizing Molecular Fishing Nets. *Phys. Today* **2018**, *71*, 40-47.

(5) Wang, L.; Boutilier, M. S. H.; Kidambi, P. R.; Jang, D.; Hadjiconstantinou, N. G.; Karnik, R. Fundamental Transport Mechanisms, Fabrication and Potential Applications of Nanoporous Atomically Thin Membranes. *Nat. Nanotechnol.* **2017**, *12*, 509–522.

(6) Park, H. B.; Kamcev, J.; Robeson, L. M.; Elimelech, M.; Freeman, B. D. Maximizing the Right Stuff: the Trade-Off between Membrane Permeability and Selectivity. *Science* **2017**, *356*, 1138–1148.

(7) Sun, Z.; Martinez, A.; Wang, F. Optical Modulators with 2D Layered Materials. *Nat. Photonics* **2016**, *10*, 227–238.

(8) Novoselov, K. S.; Mishchenko, A.; Carvalho, A.; Castro Neto, A. H. 2D Materials and van der Waals Heterostructures. *Science* **2016**, *353*, 461.

(9) Yang, F.; Cheng, S.; Zhang, X.; Ren, X.; Li, R.; Dong, H.; Hu, W. 2D Organic Materials for Optoelectronics Applications. *Adv. Mater.* **2018**, *30*, 1–27.

(10) Kissel, P.; Erni, R.; Schweizer, W. B.; Rossell, M. D.; King, B. T.; Bauer, T.; Götzinger, S.; Schlüter, a. D.; Sakamoto, J. A Two-Dimensional Polymer Prepared by Organic Synthesis. *Nat. Chem.* **2012**, *4*, 287–291.

(11) Kissel, P.; Murray, D. J.; Wulftange, W. J.; Catalano, V. J.; King, B. T. A Nanoporous Two-Dimensional Polymer by Single-Crystal-to-Single-Crystal Photopolymerization. *Nat. Chem.* **2014**, *6*, 774–778.

(12) Bhola, R.; Payamyar, P.; Murray, D. J.; Kumar, B.; Teator, A. J.; Schmidt, M. U.; Hammer, S. M.; Saha, A.; Sakamoto, J.; Schlüter, A. D.; King, B. T. A Two-Dimensional Polymer from the Anthracene Dimer and Triptycene Motifs. *J. Am. Chem. Soc.* **2013**, *135*, 14134–14141.

(13) Kory, M. J.; Wörle, M.; Weber, T.; Payamyar, P.; van de Poll, S. W.; Dshemuchadse, J.; Trapp, N.; Schlüter, A. D. Gram-Scale Synthesis of Two-Dimensional Polymer Crystals and Their Structure Anaylysis by X-Ray Diffraction. *Nat. Chem.* **2014**, *6*, 779–784.

(14) Lange, R. Z.; Hofer, G.; Weber, T.; Schlüter, A. D. A Two-Dimensional Polymer Synthesized through Topochemical [2+2]-Cycloaddition on the Multigram Scale. *J. Am. Chem. Soc.* **2017**, *139*, 2053–2059.

(15) Payamyar, P.; Kaja, K.; Ruiz-Vargas, C.; Stemmer, A.; Murray, D. J.; Johnson, C. J.; King, B. T.; Schiffmann, F.; Vandevondele, J.; Renn, A.; Götzinger, S.; Ceroni, P.; Schütz, A.; Lee, L.-T.; Zheng, Z.; Sakamoto, J.; Schlüter, A. D. Synthesis of a Covalent Monolayer Sheet by Photochemical Anthracene Dimerization at the Air/Water Interface and Its Mechanical Characterization by AFM Indentation. *Adv. Mater.* **2014**, *26*, 2052–2058.

(16) Murray, D. J.; Patterson, D. D.; Payamyar, P.; Bhola, R.; Song, W.; Lackinger, M.; Schlüter, A. D.; King, B. T. Large Area Synthesis of a Nanoporous Two-Dimensional Polymer at the Air/Water Interface. *J. Am. Chem. Soc.* **2015**, *137*, 3450–3453.

(17) Dai, W.; Shao, F.; Szczerbiński, J.; McCaffrey, R.; Zenobi, R.; Jin, Y.; Schlüter, A. D.; Zhang, W. Synthesis of a Two-Dimensional Covalent Organic Monolayer through Dynamic Imine Chemistry at the Air/Water Interface. *Angew. Chem. Int. Ed.* **2016**, *55*, 213–217.

(18) Chen, Y.; Li, M.; Payamyar, P.; Zheng, Z.; Sakamoto, J.; Schlüter, A. D. Room Temperature Synthesis of a Covalent Monoalyer Sheet at Air/Water Interface Using a Shape-Persistent Photoreactive Amphiphilic Monomer. *ACS Macro Lett.* **2014**, *3*, 153–158.

(19) Müller, V.; Shao, F.; Baljozovic, M.; Moradi, M.; Zhang, Y.; Jung, T.; Thompson, W. B.; King, B. T.; Zenobi, R.; Schlüter, A. D. Structural Characterization of a Covalent Monolayer Sheet Obtained by Two-Dimensional Polymerization at an Air/Water Interface. *Angew. Chem. Int. Ed.* **2017**, *56*, 15262–15266.

(20) Payamyar, P.; Schlüter, A. D. 2D Polymer Synthesis by Photopolymerization at the Air/Water Interface. *Encycl. Interfacial Chem.* **2018**, 181–194.

(21) Opilik, L.; Payamyar, P.; Szczerbinsk, J.; Schutz, A. P.; Servalli, M.; Hungerland, T.; Schluter, A. D.; Zenobi, R. Minimally Invasive Characterization of Covalent Monolayer Sheets Using Tip-Enhanced Raman Spectroscopy. *ACS Nano* **2015**, *9*, 4252–4259.

(22) Shao, F.; Müller, V.; Zhang, Y.; Schlüter, A. D.; Zenobi, R. Nanoscale Chemical Imaging of Interfacial Monolayers by Tip-Enhanced Raman Spectroscopy. *Angew. Chem. Int. Ed.* **2017**, *56*, 9361–9366.

(23) Makiura, R.; Konovalov, O. Interfacial Growth of Large-Area Single-Layer Metal-Organic Framework Nanosheets. *Sci. Rep.* **2013**, *3*, 1–8.

(24) Sahabudeen, H.; Qi, H.; Glatz, B. A.; Tranca, D.; Dong, R.; Hou, Y.; Zhang, T.; Kuttner, C.; Lehnert, T.; Seifert, G.; Kaiser, U.; Fery, A.; Zheng, Z.; Feng, X. Wafer-Sized Multifunctional Polyimine-Based Two-Dimensional Conjugated Polymers with High Mechanical Stiffness. *Nat. Commun.* **2016**, *7*, 13461.

(25) Kambe, T.; Sakamoto, R.; Hoshiko, K.; Takada, K.; Miyachi, M.; Ryu, J.; Sasaki, S.; Kim, J.; Nakazato, K.; Takata, M.; Nishihara, H. π-Conjugated Nickel Bis(dithiolene) Complex Nanosheet. *J. Am. Chem. Soc.* **2013**, *135*, 2462–2465.

(26) Müller, V.; Hinaut, A.; Moradi, M.; Baljozovic, M.; Jung, T. A.; Shahgaldian, P.; Möhwald, H.; Hofer, G.; Kröger, M.; King, B. T.; Meyer, E.; Glatzel, T.; Schlüter, A. D. A Two-Dimensional Polymer Synthesized at the Air/Water Interface. *Angew. Chem. Int. Ed.* **2018**, *57*, 1–6.

(27) Müller, V.; Hungerland, T.; Baljozovic, M.; Jung, T.; Spencer, N. D.; Eghlidi, H.; Payamyar, P.; Schlüter, A. D. Ink-Free Reversible Optical Writing in Monolayers by Polymerization of a Trifunctional Monomer: Toward Rewritable 'Molecular Paper'. *Adv. Mater.* **2017**, *29*, 1701220.

(28) Bauer, T.; Zheng, Z.; Renn, A.; Enning, R.; Stemmer, A.; Sakamoto, J.; Schlüter, A. D. Synthesis of Free-Standing, Monolayered Organometallic Sheets at the Air/Water Interface. *Angew. Chem. Int. Ed.* **2011**, *50*, 7879–7884.

(29) Zheng, Z.; Ruiz-vargas, C. S.; Bauer, T.; Rossi, A.; Payamyar, P.; Schütz, A.; Stemmer, A.; Sakamoto, J.; Schlüter, A. D. Square-Micrometer-Sized, Free-Standing Organometallic Sheets and Their Square-Centimeter-Sized Multilayers on Solid Substrates. *Macromol. Rapid Commun.* **2013**, *34*, 1670–1680.

(30) Yu, C.; Jin, Y.; Zhang, W. Two-Dimensional Polymer Synthesis by Dynamic Chemistry at the Air–Water Interface. *Encycl. Interfacial Chem.* **2018**, 486–498.

(31) Sakamoto, R.; Hoshiko, K.; Liu, Q.; Yagi, T.; Nagayama, T.; Kusaka, S.; Tsuchiya, M.; Kitagawa, Y.; Wong, W.-Y.; Nishihara, H. A Photofunctional Bottom-Up Bis(dipyrrinato)zinc(II) Complex Nanosheet. *Nat. Commun.* **2015**, *6*, 6713.

(32) Hofer, G.; Grieder, F.; Kröger, M.; Schlüter, A. D.; Weber, T. Unraveling Two-Dimensional Polymerization in the Single Crystal. *J. Appl. Crystallogr.* **2018**, *51*, 481–497.

(33) Odian, G. *Principles of Polymerization*; John Wiley & Sons, NJ, USA, 2004.

(34) Lu, C.; Lipson, L. P. Interference Lithography: a Powerful Tool for Fabricating Periodic Structures. *Laser Photonics Rev.* **2010**, *4*, 568–580.

(35) Rothschild, M.; Bloomstein, T. M.; Kunz, R. R.; Liberman, V.; Switkes, M.; Palmacci, S. T.; Sedlacek, J. H. C.; Hardy, D.; Grenville, A. Liquid Immersion Lithography: Why, How, and When? *J. Vac. Sci. Technol. B Microelectron. Nanom. Struct.* **2004**, *22*, 2877–2881.

(36) Pan, L.; Park, Y.; Xiong, Y.; Ulin-Avila, E.; Wang, Y.; Zeng, L.; Xiong, S.; Rho, J.; Sun, C.; Bogy, D. B.; Zhang, X. Maskless Plasmonic Lithography at 22 nm Resolution. *Sci. Rep.* **2011**, *1*, 1–6.

(37) Dunn, R. C. Near-Field Scanning Optical Microscopy. *Chem. Rev.* **1999**, *99*, 2891–2928.

(38) Servalli, M.; Trapp, N.; Wörle, M.; Klärner, F. G. Anthraphane: An Anthracene-Based, Propeller-Shaped D_{3h}-Symmetric Hydrocarbon Cyclophane and Its Layered Single Crystal Structures. *J. Org. Chem.* **2016**, *81*, 2572–2580.

(39) Servalli, M.; Trapp, N.; Schlüter, A. D. Single-Crystal-to-Single-Crystal (SCSC) Linear Polymerization of a Desymmetrized Anthraphane. *Chem. Eur. J.* **2018**, *24*, 15003-15012.

(40) Servalli, M.; Trapp, N.; Solar, M.; Schlüter, A. D. Library of Single Crystal Structures of a D_{3h}-Symmetric Hydrocarbon Cyclophane: A Comprehensive Packing Study of Anthraphane from 30 Solvents. *Cryst. Growth Des.* **2017**, *17* , 3419-3432.

(41) Servalli, M.; Solar, M.; Trapp, N.; Wörle, M.; Schlüter, A. D. Photochemical Single-Crystal-to-Single-Crystal (SCSC) Reactions of Anthraphane to Dianthraphane and $Poly_{1D}$ anthraphane. *Cryst. Growth Des.* **2017**, *17*, 6510–6522.

(42) Hennrich, G. Synthesis and Spectroscopic Properties of 1,3,5-Tris(arylalkynyl)-2,4,6-trimethoxybenzenes. *Tetrahedron* **2004**, *60*, 9871–9876.

(43) Wenk, H. H.; Sander, W. Generation of Fluorinated *m*-Benzyne Derivatives in Neon Matrices. *Eur. J. Org. Chem* **2002**, *23*, 3927–3935.

(44) Fu, G. C. The Development of Versatile Methods for Palladium-Catalyzed Coupling Reactions of Aryl Electrophiles through the Use of P(*t*-Bu)3 and PCy3 as Ligands. *Acc. Chem. Res.* **2008**, *41*, 1555–1564.

(45) Klamt, A.; Schüürmann, G. COSMO: A New Approach to Dielectric Screening in Solvents With Explicit Expressions for the Screening Energy and Its Gradient. *J. Chem. Soc. Perkin Trans. 2* **1993**, 5, 799–805.

(46) Hayashi, T.; Mataga, N.; Sakata, Y.; Misumi, S.; Morita, M.; Tanaka, J. Excimer Fluorescence and Photodimerization of Anthracenophanes and 1,2-Dianthrylethanes. *J. Am. Chem. Soc.* **1976**, *98*, 5910–5913.

(47) Bouas-Laurent, H.; Desvergne, J.-P.; Castellan, A.; Lapouyade, R. Photodimerization of Anthracenes in Fluid Solution: Structural Aspects. *Chem. Soc. Rev.* **2000**, *29*, 43–55.

(48) Bouas-Laurent, H.; Desvergne, J.-P.; Castellan, A.; Lapouyade, R. Photodimerization of Anthracenes in Fluid Solution: (Part 2) Mechanistic Aspects of the Photocycloaddition and of the Photochemical and Thermal Cleavage. *Chem. Soc. Rev.* **2001**, *30*, 248–263.

(49) Fudickar, W.; Fery, A.; Linker, T. Reversible Light and Air-Driven Lithography by Singlet Oxygen. *J. Am. Chem. Soc.* **2005**, *127*, 9386–9387.

(50) Fudickar, W.; Linker, T. Remote Substituent Effects on the Photooxygenation of 9,10-Diarylanthracenes: Strong Evidence for Polar Intermediates. *Chem. Commun.* **2008**, 1771–1773.

(51) Fudickar, W.; Linker, T. Novel Anthracene Materials for Applications in Lithography and Reversible Photoswitching by Light and Air. *Langmuir* **2010**, *26*, 4421–4428.

(52) Feng, S.; Sen, P. N. Percolation on Elastic Networks: New Exponent and Threshold. *Phys. Rev. Lett.* **1984**, 52, 216–219.

(53) Li, M.; Schlüter, A. D.; Sakamoto, J. Solid-State Photopolymerization of a Shape-Persistent Macrocycle with two 1,8-Diazaanthracene Units in a Single Crystal. *J. Am. Chem. Soc.* **2012**, *134*, 11721–11725.

(54) Servalli, M.; Gyr, L.; Sakamoto, J.; Schlüter, A. D. Propeller-Shaped D_{3h}-Symmetric Macrocycles with Three 1,8-Diazaanthracene Blades as Building Blocks for Photochemically Induced Growth Reactions. *Eur. J. Org. Chem.* **2015**, *20*, 4519–4523.

(55) Zhao, Y.; Bernitzky, R. H. M.; Kory, M. J.; Hofer, G.; Hofkens, J.; Schlüter, A. D. Decorating the Edges of a 2D Polymer with a Fluorescence Label. *J. Am. Chem. Soc.* **2016**, *138*, 8976–8981.

(56) Leggett, G. Light-Directed Nanosynthesis: Near-field Optical Approaches to Integration of the Top-down and Bottom-up Fabrication Paradigms. *Nanoscale* **2012**, *4*, 1840-1855.

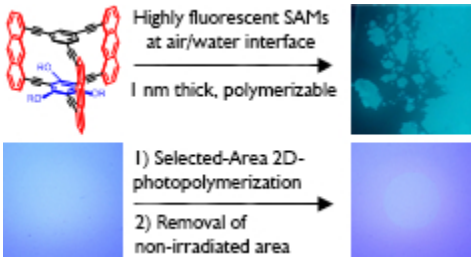

TOC

82x44mm (72 x 72 DPI)